Available online at www.sciencedirect.com
SCIENCE DIRECT
Talanta 68 (2006) 700–707
Talanta
www.elsevier.com/locate/talanta

A method for DNA detection in a microchannel: Fluid dynamics phenomena and optimization of microchannel structure

Y. Yamaguchi [a], D. Ogura [a], K. Yamashita [a], M. Miyazaki [a,b], H. Nakamura [a], H. Maeda [a,b,*]

[a] *National Institute of Advanced Industrial Science and Technology (AIST), Micro-space Chemistry Laboratory, 807-1, Shuku, Tosu 841-0052, Japan*
[b] *Graduate School of Engineering Sciences, Kyushu University, 6-1, Kasuga-Kouen, Kasuga 816-8580, Japan*

Received 15 November 2004; received in revised form 12 May 2005; accepted 12 May 2005
Available online 20 June 2005

Abstract

A simple DNA diagnosis method using microfluidics has been developed which requires simple and straightforward procedures such as injection of sample and probe DNA solutions. This method takes advantage of the highly accurate control of fluids in microchannels, and is superior to DNA microarray diagnosis methods due to its simplicity, highly quantitative determination, and high-sensitivity. The method is capable of detecting DNA hybridization for molecules as small as a 20 mer. This suggests the difference in microfluidic behavior between single strand DNA (ssDNA) and double stranded DNA (dsDNA). In this work, influence of both the inertial force exerted on DNA molecules and the diffusion of DNA molecules was investigated. Based on the determination of these parameters for both ssDNA and dsDNA by experiments, a numerical model describing the phenomena in the microchannel was designed. Computational simulation results using this model were in good agreement with previously reported experimental results. The simulation results showed that appropriate selection of the analysis point and the design of microchannel structure are important to bring out the diffusion and inertial force effects suitably and increase the sensitivity of the detection of DNA hybridization, that is, the analytical performance of the microfluidic DNA chip.

Keywords: DNA diagnosis; Microchannel; Microreactor; Microfluidics; Computational fluid dynamics simulation

1. Introduction

Demand for the on-site detection of genes has increased rapidly in pathophysiological examinations in clinical laboratories. DNA micro arrays, which are currently in widespread use, enable the diagnosis of many samples at a time. However, high-throughput screening is not always a priority in clinical diagnostics. To satisfy the demand for the accurate diagnosis of some specific genetic diseases, a method capable of providing high-accuracy, simplicity, and high-quantity, rather than high-throughput would be desirable [1]. The micro total analysis system (μTAS) represents a suitable solution to the above problem [2,3]. Microchannels, which are essential components of μTAS devices, play two important roles; one of which is to minimize the amount of sample and the device volume, and the other is their high-controllability of microfluids. The fluid in microchannels forms stable laminar flow, which does not include turbulence components because of its low Reynolds number. This property holds the promise of a reproducible and highly accurate analysis. Several microdevices which utilize such excellent aspect of microfluidics have been reported. They are applied for biochemical analysis or particle separation taking advantage of accurate control of diffusion and fluid flow [4–6]. Microdevices have been also applied for DNA diagnosis. Several DNA diagnosis devices which utilize microchannels have been reported which include the use of microelectrophoresis [7,8] or components with an elaborate structure [9]. A simpler method involving a different concept has also been proposed [10]. The method enables the analysis of even single nucleotide polymorphisms (SNPs) by injecting target DNA and probe DNA solutions into a simple serpentine microchannel. Since this device is highly accurate and sim-

* Corresponding author. Tel.: +81 942 81 3676; fax: +81 942 81 3657.
E-mail address: maeda-h@aist.go.jp (H. Maeda).

0039-9140/$ – see front matter © 2005 Elsevier B.V. All rights reserved.
doi:10.1016/j.talanta.2005.05.010

ple, it promises to be useful in medical laboratories. The device also offers an advantage of ease of fabrication due to its simple microchannel structure. Nevertheless, it involves several properties such as length of channel, curvature radius, aspect ratio of the cross-section plane of the channel, and fluid velocity. Optimization of these properties makes it possible to improve the sensitivity of this microfluidic DNA chip. The purpose of this work was to clarify the principle of this analysis by computational simulation of DNA fluid dynamics in a microchannel, and to pave the way for optimization of the microchannel structure.

The characteristics of this microfluidic DNA analysis chip are as follows. The sample DNA solution and FITC-labeled probe DNA solution are injected into the two inlets (inlet a and b in Fig. 1), respectively. The two solutions pass through the microchannel which contains several curves, forming side-by-side laminar flows. The fluorescence intensity is measured at the side of the sample DNA (the side of inlet a), that is, the amount of probe DNAs that spread into the side of the sample DNA is measured. It has been reported that the fluorescence intensity is larger under the condition where the sample and probe DNAs hybridized, in contrast to the absence of hybridization. To further explain this observation, diffusion efficiency should be considered first. However, the increasing degree of fluorescence intensity has different features between after an odd-number turns (point B or D in Fig. 1) compared to after an even-number turns (point C or E) [10]. This suggests that the principle of DNA analysis involves not only diffusion, but also the influence of the curves in the microchannels.

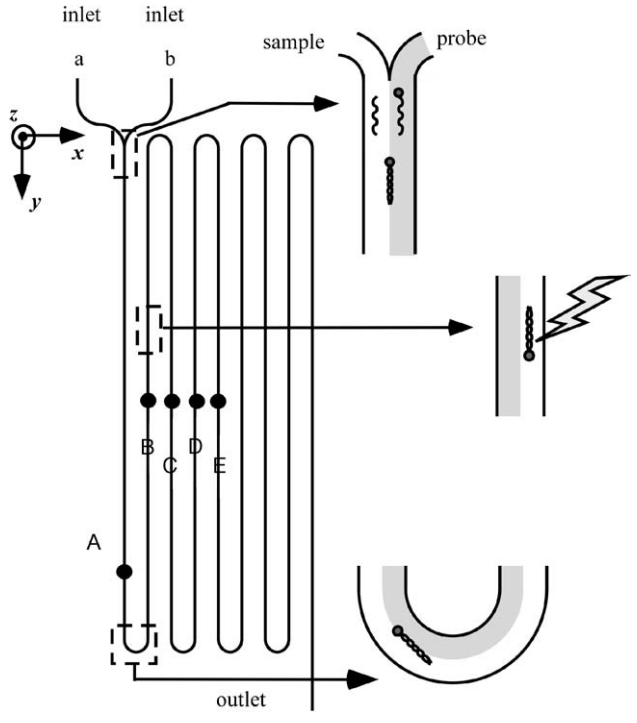

Fig. 1. Structure of a microfluidic DNA analysis chip. The target DNA and the FITC-labeled probe DNA solutions are injected into inlets a and b, respectively.

It has been shown that inertial force is exerted on the fluids at a curve in the microchannel by computational fluid dynamics simulation [11,12], the three-dimensional observation of microfluid [11], and micro sphere classification experiments [12]. This suggests that the inertial force is also exerted on the solute, and the trajectory thrusts outward at the curve. Heavier molecules would be moved to the periphery in preference to lighter molecules due to the stronger inertial force. This effect could change the behavior of DNA before and after hybridization. However, an explanation of the different results after odd and even number turns is not currently available. In this work, the influence of repeated microchannel curves on the behavior of DNA molecules was evaluated by computational fluid dynamics and observation using confocal fluorescence microscopy. Results provide some new information relative to the principle of the microfluidic DNA analysis chip. These findings herein offer some guidelines for the design of the microchannel structure.

2. Model for the behavior of hybridized DNA

The ssDNA molecules that are injected into the two inlets of the microchannels encounter each other on a stable "differential medium laminar interface", which is formed at the center of the microchannel. The dsDNAs are formed at this location if they are complementary. DNAs on the interface diffuse in accordance to their intrinsic diffusion coefficient as they pass through the straight channels. DNAs at the channel center ($y = 0$ in Fig. 1) are distributed according to the following equation [13],

$$p(x,t) = C\frac{\exp(-x^2/4Dt)}{\sqrt{4\pi Dt}}, \quad (1)$$

where C is a constant corresponding to the amount of DNA, x is the position transverse to the flow (cf. Fig. 1), D is the diffusion coefficient, and t the diffusion time. The value for C is determined by the concentration of the DNA solution and speed of hybridization. Let C be equal to unity here, considering $p(0,0)$ as unity, that is, being a relative value. The equation follows a normal distribution.

DNA molecules that are distributed according to the Eq. (1) might be forced by inertial force at the curve. It has generally been considered that body force such as inertial force can be neglected compared with surface force since the surface area per volume is extremely large in microchannels. However, computational simulation and direct observation [11], and experimental results of microparticle classification [12] indicate that inertial force is exerted in reality and influences fluidic behavior. The inertial force in the channel yields one pair of vortices termed Dean vortices (Fig. 3). DNA molecules are carried on these Dean vortices. The

DNA molecules at the merging point ($y = 0$) pass through the microchannel changing their distribution by repetition of such transfer and diffusion. This can be described by the equations below. The DNA distribution before a turn in a curve can be explained using the residence time t_0 and Eq. (1) as follows:

$$q_0(x, z) \cong p(x, t_0(z)) = \frac{\exp(-x^2/4Dt_0(z))}{\sqrt{4\pi Dt_0(z)}}. \quad (2)$$

Since the velocity profile in the microchannel is not uniform, t_0 is a function of the depth position z. Meanwhile, after the first turn, the peak of the distribution shifts by $\Delta x(z)$ because of the inertial force, where Δx is a function of depth, z (cf. Fig. 3). Therefore,

$$q_1(x, z) \cong p(x - \Delta x(z), t_1(z)) = \frac{\exp(-(x - \Delta x(z))^2/4Dt_1(z))}{\sqrt{4\pi Dt_1(z)}} \quad (3)$$

In previously reported methods, microspectrophotometry was used to measure the amount of dsDNA [10]. In this method, a microchannel is irradiated with an Ar laser above the top wall and the fluorescence intensity that is produced throughout the channel depth is measured. Therefore, the observed fluorescence intensity can be estimated by accumulating $q_i(x,z)$ throughout the whole z, that is, by the following equation

$$Q_i(x) = \sum_z q_i(x, z) \quad (4)$$

corresponding to data collected by microspectrophotometry.

In addition, DNA hybridization continues to occur near the interface as DNA passes through the channel. Finally, considering such an increase in dsDNA for each turning, its distribution after the nth turn can be roughly estimated as follows:

$$R_{n\_\mathrm{dsDNA}}(x) = \sum_i^n Q_i(x). \quad (5)$$

In reported experiments, the value $R_{n\_\mathrm{dsDNA}}(x)$ from which $R_{n\_\mathrm{ssDNA}}(x)$ was subtracted as a control increased with increasing number of turns, where $R_{n\_\mathrm{ssDNA}}(x)$ is distribution profile of ssDNA near the center of the channel in the condition that DNAs are not complementary. That is, $R_{n\_\mathrm{ssDNA}}(x)$ is the amount of single strand DNA which might have hybridized if DNAs are complementary. Regardless of DNAs being complementary or not, surplus ssDNAs exist across nearly half of the channel. Because the amount of the surplus ssDNAs including diffusion and inertial force effects should be the same, the difference of DNA distribution between the hybridizing/non-hybridizing conditions corresponds to the difference between $R_{n\_\mathrm{dsDNA}}(x)$ and $R_{n\_\mathrm{dsDNA}}(x)$. This paper attempts to describe the fluid dynamics phenomenon of DNA detection in a microfluidic system using the above numerical model. The parameters in the model such as diffusion coefficient D were estimated both experimentally and by computation methods. The estimation and validation of this model using these parameters are described in detail in the results and discussion section.

The above description is applicable when the fluid velocity is relatively small. In this work, the fluid velocity is about 30 mm/s and the Dean number is about 3.5. Such a small Dean number implies weak Dean vortices. Therefore, fluid movement along the z-axis (depth direction) can be neglected. For that reason, we consider only the fluid movement that occurs along the x-axis (in the horizontal plane).

3. Experimental

A confocal fluorescence microscopy system (Nikon, Japan) was used to investigate the fluidic behavior of the DNA solution and molecules in a three-dimensional manner. Microchannels were fabricated mechanically on acrylic plates (3 cm × 7 cm) as reported in a previous paper [14]. The cross-sectional plane of the channel was 300 μm in width and 200 μm in depth. Straight channels (length = 52 mm) and half circular arcs (curvature radius = 1.0 mm) were connected repeatedly. Two types of 20 mer DNA, which are complementary to each other, were obtained from Qiagen K. K. (Japan). One of the DNAs was labeled with FITC at the 5′ end serving as the probe DNA (Fig. 2). The other served as the target DNA. The molecular weights before and after hybridization were estimated to be 7000 and 14,000, respectively. Probe and target DNA solutions each equivalent to 500 nM were injected into the microfluidic DNA analysis chip at a flow rate of 30 mm/s using a programmable syringe pump (Kd Scientific Inc., USA).

For the numerical elucidation of the phenomena, the distribution of fluid velocity in the microchannel was calculated using FLUENT 6.1 (Fluent Inc., USA) based on a finite-volume scheme. The cross-sectional plane was divided into 60 × 40 mesh sections. The curved portion of the channel in the shape of a semicircle was divided in 1.5° segments (120 meshes). The total number of mesh sections in the calculated space was 432,000. The value of $\Delta x(z)$ for each turn was calculated by time integration of the velocity vectors at each mesh and by multiplying them by a constant so as to they correspond to the observed $\Delta x(z)$ after the first turn.

4. Results and discussion

The diffusion coefficients D for 20 mer ssDNA and dsDNA were first estimated. FITC-labeled ssDNA or the dsDNA solution and phosphate buffer were injected into the two inlets to form two-layered laminar flow with an average flow rate of 30 mm/s.

The solid lines in Fig. 2(a) correspond to the fluorescence intensity profile at point A in Fig. 1 ($y = 40$ mm) at the central

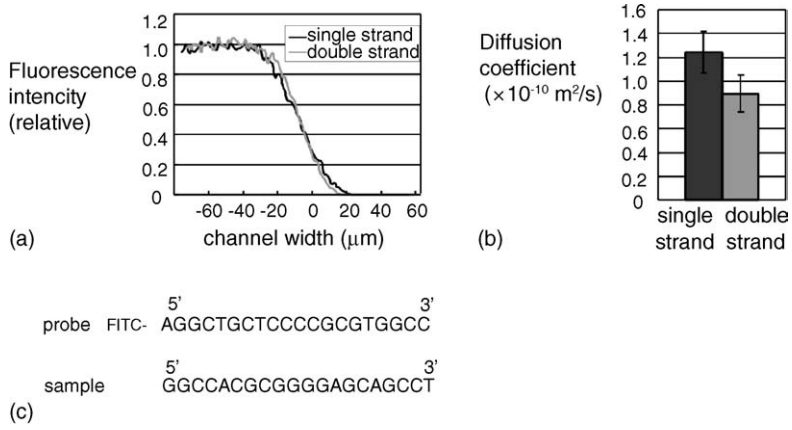

Fig. 2. Estimation of diffusion coefficients D for ssDNA and dsDNA. (a) Fluorescence intensity profiles at point A in Fig. 1 ($y = 40$ mm). (b) Values of D were estimated by curve fitting. (c) Structures of probe and sample DNAs used in this study.

depth ($z = 0$). This distribution obeys the following equation [8],

$$C(x) = \frac{1}{2}\left\{1 - \mathrm{erf}\left(\frac{x}{2\sqrt{Dt}}\right)\right\}, \quad (6)$$

where erf(·) is the error function which is similar to the sigmoid function. The diffusion time is roughly estimated as y/U_{max} where $|x|$ is extremely small. Theoretically, U_{max} is about twice the average velocity U_{ave} (30 mm/s) and this was also confirmed by calculation using the FLUENT program. Thus, D was estimated by fitting Eq. (6) to the observed data (Fig. 2b). The values of D for ssDNA and dsDNA were estimated to be 1.2×10^{-10} and 0.89×10^{-10} (m^2/s), respectively. These values were the average of nine observations. These values are considered to be fairly valid from the view point of the order, compared to the reported value for Lysozyme (Mw = 14,100), 1.04×10^{-10} (m^2/s) [15] and for a 39 mer ssDNA, 0.44×10^{-10} (m^2/s) [16]. The D of dsDNA is smaller because dsDNA is larger in size compared to ssDNA. The value of D for dsDNA was slightly smaller than the value predicted by the Stokes–Einstein relation [15] and by assuming a spherical shape for dsDNA (0.95×10^{-10}(m^2/s)). Fig. 3a shows the dsDNA distribution at point A, which has diffused according to the estimated D.

Inertial force is exerted on the DNA distribution at a curve. Fig. 3b shows that the center for the distributed ssDNA and dsDNA is shifted outward near the central depth ($z = 0$ μm) and inward near the top and bottom of the wall ($z = \pm 100$ μm). The values of the shifts are the average of three observations using fluorescence confocal microscopy. Although the difference between ssDNA and dsDNA is small (4.2 μm), it is larger than the resolution of fluorescence confocal microscopy (1.4 μm). In order to compare this difference in the curved channel with the noise level of the spatial measurements, interface position of a stable two laminar flow (30 mm/s) in a straight channel was measured. The average of the noise was about 1.9 μm, which was significantly less than the above difference ($p < 0.05$, t-test). After the second turn, the inertial force in the opposite direction moves the shifts back to around $x = 0$. Fig. 3c shows the observed position of the center of distribution. The line is not absolutely straight because of the non-uniform strength of the inertial force. Simulation results indicated that the displacement is larger for dsDNA than for ssDNA and the difference increases with the number of turns, although this difference is extremely small (Fig. 3d). Thus, the distribution of DNA changes its peak position along x axis, becoming broader with time. Fig. 4 shows simulated results for the accumulated distribution through the entire depth, that is, represented by $Q_i(x)$ where $i = 1$–8. After an odd number of turns, the distribution is asymmetric because the peak position for the distribution, $\Delta x(z)$, is different with depth. While, it is nearly symmetric after an even number of turns because $\Delta x(z)$s are assembled on the y axis, and thus, the difference between ssDNA and dsDNA becomes large.

Fig. 5a and b show $R_{n\_ssDNA}(x)$ and $R_{n\_dsDNA}(x)$ ($n = 1$–8) in Eq. (5), respectively. Fig. 5c and d indicates the difference between them, $\Delta R(x) = R_{n\_dsDNA}(x) - R_{n\_ssDNA}(x)$. The profiles are completely different for even versus odd turns, and this difference becomes larger after the eighth turn.

If a laser irradiates at a distance of 20 μm from the center ($x = -20$ μm) and the spot diameter of the observation is about 40 μm, the observed fluorescence intensity corresponds to the summation of the values in the shaded regions in Fig. 5c and d. The values are shown in Fig. 6a. The values after the second and fourth turns are larger than for the first and third turns. In addition, the values become larger with increasing number of turns. These results are in good agreement with the experimental results [10]. The numerical model mentioned above attempts to explain the principles behind the DNA microfluidic analysis method.

It is the balance of the inertial force and diffusion that yields the above described tendency. First, it is important that the diffusion coefficient be different between ssDNA and dsDNA. This difference leads to the localization of dsDNA around the center of the channel. Second, since the peak positions after an odd number of turns are different among the channel depth as described in Eq. (3), the distribution of

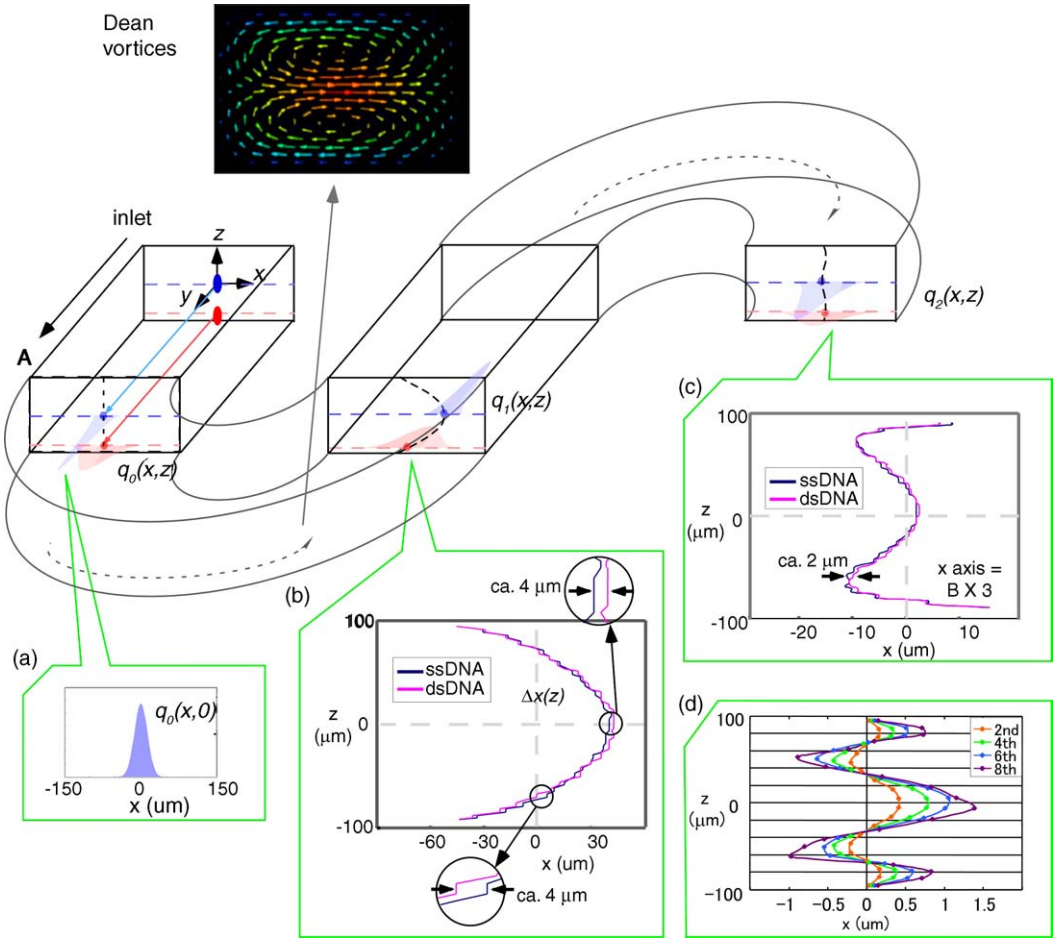

Fig. 3. Diagrammatic illustration of the variation in DNA distribution as the DNA passes through the curved microchannel. Mathematical expressions in the figure correspond to Eqs. (2) and (3). (a) DNAs that are at the position $x = y = z = 0$ follow a normal distribution before the first turn. (b) Shifts in the peak of the distribution due to inertial force after the first turn. Double stranded DNA (dsDNA) thrusts more outward than single strand DNA (ssDNA). (c) After the second turn, the center of the distribution is located near the back center of the channel. (d) Simulated results of the difference between dsDNA and ssDNA in Fig. 3c.The difference increases with the number of turns.

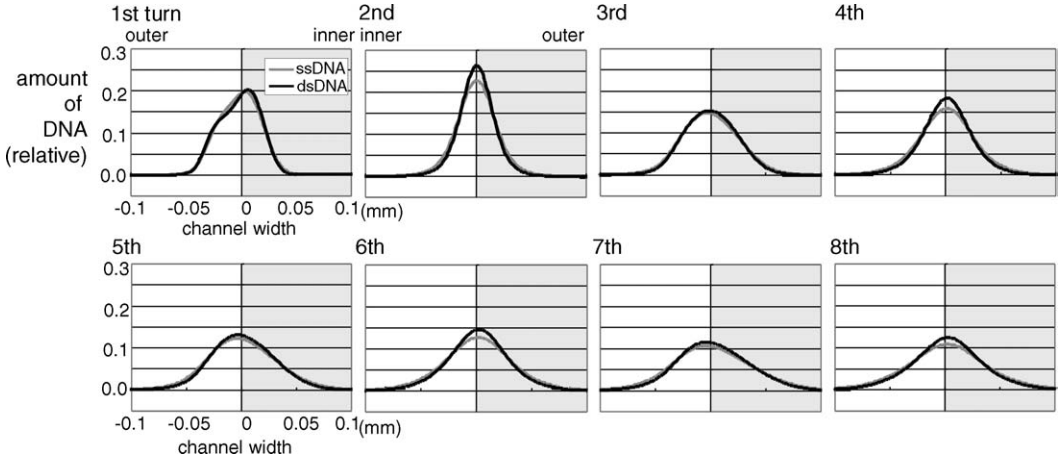

Fig. 4. Transformation of DNA distribution accumulated through the entire depth. Distribution is different between ssDNA and dsDNA particularly after an even number of turns.

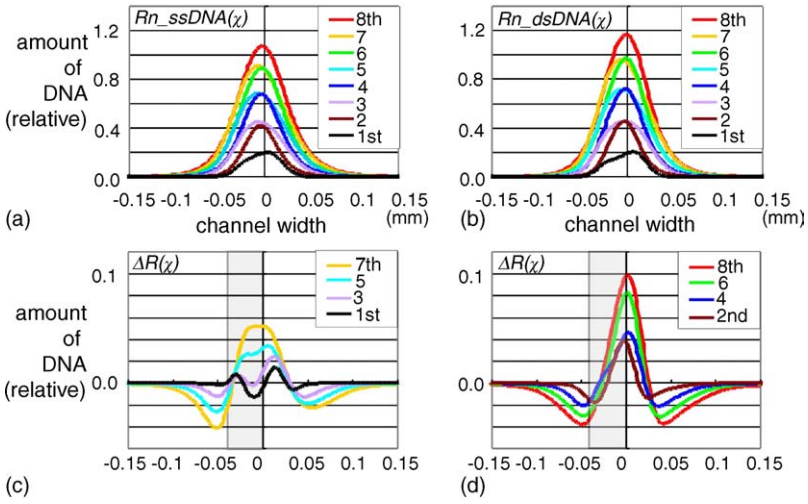

Fig. 5. DNA distribution accumulated along the channel depth. (a) and (b) shows ssDNA and dsDNA distribution, respectively. (c) and (d) indicates $\Delta R(x)$, computed from the subtraction of (b) from (a). (c) is $\Delta R(x)$ after an odd number of turns, while (d) is $\Delta R(x)$ after an even number of turns.

$\Delta R(x)$ becomes bimodal after an odd number of turns. On the other hand, $\Delta R(x)$ becomes unimodal after an even number of turns because all the peak positions assemble near the center of the channel. Such difference in the DNA distribution between the odd and even numbers of turns causes the large difference in fluorescence intensity.

Our previous paper reported that a longer target DNA yields a larger difference [5]. In order to investigate whether the above model can be used to explain such a phenomenon, a dsDNA with twice the molecular weight and volume was assumed. Considering that the inertial force should increase, the difference of $\Delta x(z)$s was doubled. The diffusion coefficient was set to $0.71 \times 10^{-10}(\mathrm{m}^2/\mathrm{s})$, approximating a spherical shape for the dsDNA for the sake of simplicity and for applying the Stokes–Einstein relation. Fig. 6b shows the new ΔR for the ssDNA and the large dsDNA. The obtained values are larger compared with Fig. 6a after an even number of turns: this tendency is in good agreement with the experimental result.

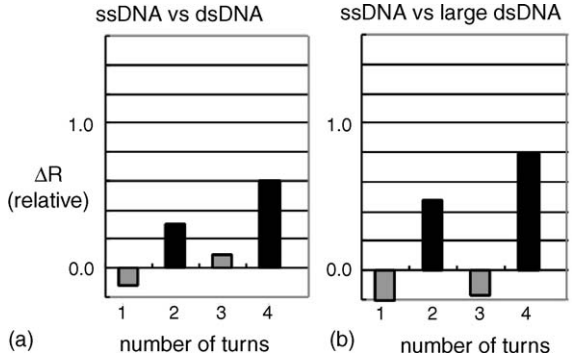

Fig. 6. Accumulated ΔR. This value corresponds to the analysis signal for the detection of hybridization. Values after an even number of turns are larger than an odd number of turns. (a) 20 mer ssDNA and dsDNA, (b) 20 mer ssDNA and 40 mer dsDNA are assumed.

Controlling effects of diffusion and inertial force is achievable through suitable selection of a microchannel structure to improve the accuracy and sensitivity of this microfluidic DNA analysis chip. For example, the length of the microchannel's straight section can control diffusion effects. The curvature radius and aspect ratio of the cross-sectional plane alter the secondary flow effects. This study examined effects of the microchannel's straight section length and the aspect ratio of the cross-sectional plane using the previously described numerical model.

Fig. 7 shows simulated ΔR values (after the fourth turn) where the straight section of the microchannel was shortened to 35 mm or lengthened to 80 mm. The results indicate that a shorter straight portion is a disadvantage in terms of improving sensitivity. To further investigate this, the following reasoning was considered. Since a shorter straight channel leads to less diffusion, the profile for DNA distribution becomes sharp as shown in Fig. 8a and b, compared with Fig. 5a and b. This clearly shows that the sharp peak distribution does not obscure the difference between the peak positions among the different depths and the distortion of the distribution caused by the inertial force. This effect causes a bimodal distribution

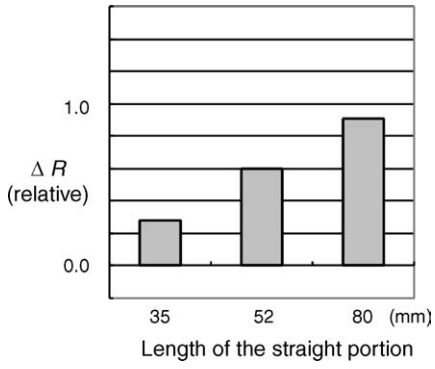

Fig. 7. Effect of the length of microchannel's straight portion on ΔR.

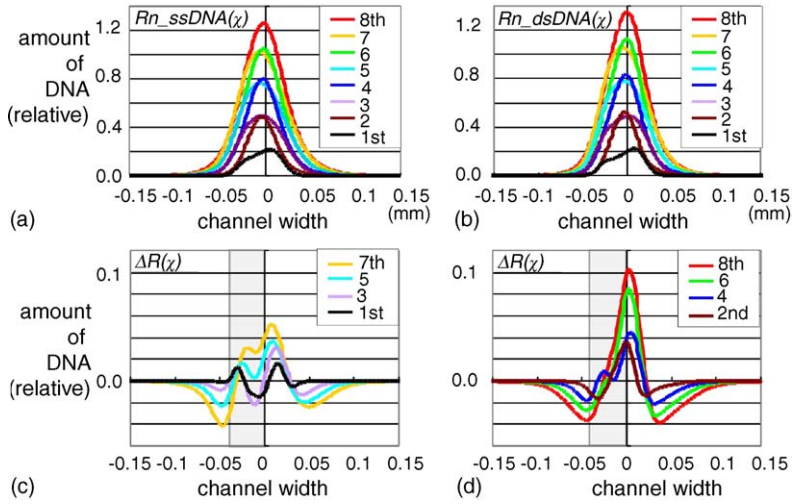

Fig. 8. DNA distribution accumulated along the channel depth where the length of the straight portion of the channel is shortened to 35 mm. (a) and (b) shows ssDNA and dsDNA distribution, respectively. (c) and (d) indicates $\Delta R(x)$, computed from the subtraction of (b) from (a). (c) is $\Delta R(x)$ after an odd number of turns, while (d) is $\Delta R(x)$ after an even number of turns.

in $\Delta R(x)$ even after the fourth turn (Fig. 8d) in addition to an odd number of turns (Fig. 8c). However, in the case of a broad distribution, the difference is less distinct. As the sharpness of the distribution is reduced during DNA solution passing through the microchannel, $\Delta R(x)$ becomes broader and unimodal after the sixth and eighth turn, resulting in a larger ΔR. In this case, it would be advantageous to detect the fluorescence intensity after the sixth turn, not the fourth turn. In this manner, analytical performance depends largely on a balance of diffusion and inertial force. This also indicates that suitable length of the straight portion of a channel depends on other structure parameter such as curvature radius, the aspect ratio of the cross-sectional plane of the microchannel and inherent restriction of the apparatus, such as the size of the laser and observation location.

Fig. 9 shows the effects of the aspect ratio of the microchannel's cross-sectional plane. For comparison, the cross-sectional area of the microchannel was made uniform at 40,000 μm^2. The ΔR value is generally larger where the microchannel width is narrower because ΔR is an accumulation of fluorescence intensity through the entire depth. However, the value was smallest where the width (and depth) is 200 μm. Distortion of the interface area was greatest where the aspect ratio is unity. It is considered that this feature reduces the ΔR value. Fig. 9 also shows the influence of the straight section length. In Fig. 9a, the longer channel generally provided larger ΔR, as shown in Fig. 7. It is important to trim the microchannel volume to reduce the amount of sample and prove DNA in practical application. Considering this problem, the total length of the microchannel was made uniform, as shown in Fig. 9b. It is difficult to extract the general tendency from these results, but results indicate that relation between the effects of diffusion and inertial force is intricate and its control is important to improve performance of analysis. This result also depends on restriction of analysis methods and apparatus, such as the laser-spot diameter and the observed positions. In the restriction in this work, the deepest microchannels or one whose

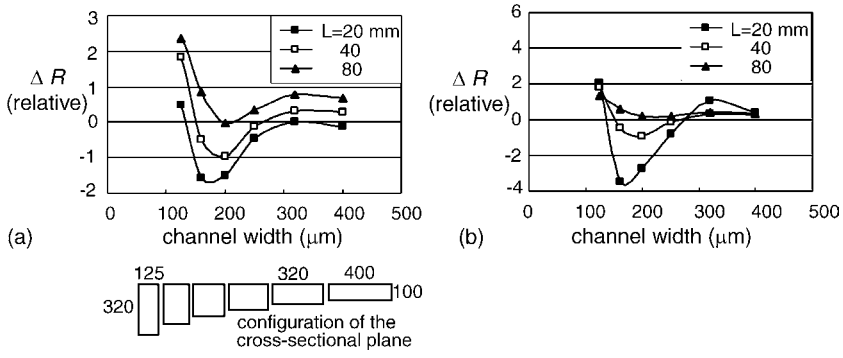

Fig. 9. Effect on ΔR of the aspect ratio of the microchannel's cross-sectional plane. The length of the microchannel's straight portion (L) was changed from 20 to 80 mm. (a) ΔR after the eighth turn. (b) The microchannel length was uniform. ΔR after the 16th, 8th, and 4th turns are shown respectively for $L = 20$, 40 and 80 mm.

width is 320 μm and $L = 20$ mm (including many turns) are better.

The microchannel in this chip follows a simple serpentine geometry. Therefore, this model can be used in other applications in chemical analysis and for separation after synthesis for enzyme-substrate complex and others. In this synthesis, the molecular weight of the product becomes larger than the reactants. To achieve higher accuracy and sensitivity, for even a simple channel structure, the microchannel must be designed to be specific and suitable for respective products and reactants within the restriction of analysis methods and apparatus. Laminar flow, which enables this microfluidic DNA analysis, also enables relatively simple calculation for design of microchannel structure and analytical methods.

5. Conclusion

This study reported a novel and simple type of microfluidic DNA analysis chip in which the sample and probe DNA solutions are merely injected into the serpentine microchannel. In this study, computational simulation was carried out by construction of a numerical model involving the analytical principles. Computational simulation results using this model showed good agreement with previously reported experimental results. Differences were found between ssDNA and dsDNA, both in the diffusion coefficient and the inertial force exerted at the microchannel turn. Those differences emphasize the success of this analysis. Despite the use of a simple serpentine microchannel, the balance of effects of the diffusion coefficient and inertial force intricately affected the analytical performance of the system. We conclude that appropriate selection of the analysis point and design of the microchannel structure are important to bring out diffusion and inertial force effects suitably and increase the detection sensitivity. A suitable detection point should be determined depending on the microchannel structure; a suitable microchannel structure should be considered under the restriction of the apparatus. The numerical model described in this paper is useful for determining the microchannel structure design and guidelines for analytical methods.

References

[1] J. Wang, Chem. Eur. J. 5 (1999) 1681–1685.
[2] M.A. Burns, B.N. Johnson, S.N. Brahmasandra, K. Handique, J.R. Webster, M. Krishnan, T.S. Sammarco, P.M. Man, D. Jones, D. Heldsinger, C.H. Mastrangelo, Science 282 (1998) 484–487.
[3] T. Chován, A. Guttman, Trends Biotechnol. 20 (2002) 116–122.
[4] B.H. Weigl, P. Yager, Science 283 (1999) 346–347.
[5] M. Yamada, M. Nakashima, M. Seki, Anal. Chem. 76 (2004) 5465–5471.
[6] F. Petersson, A. Nilsson, H. Jönsson, T. Laurell, Anal. Chem. 77 (2005) 1216–1221.
[7] H. Wang, J. Qin, Z. Dai, L. Wang, J. Bai, B. Lin, J. Sep. Sci. 26 (2003) 869–874.
[8] G.-B. Lee, S.-H. Chen, G.-R. Huang, W.-C. Sung, Y.-H. Lin, Sens. Actuators B 75 (2001) 142–148.
[9] L.R. Huang, Anal. Chem. 75 (2003) 6963–6967.
[10] K. Yamashita, Y. Yamaguchi, M. Miyazaki, H. Nakamura, H. Shimizu, H. Maeda, Lab Chip 4 (2004) 1–3.
[11] Y. Yamaguchi, F. Takagi, K. Yamashita, H. Nakamura, H. Maeda, K. Sotowa, K. Kusakabe, Y. Yamasaki, S. Morooka, Chem. Eng. J. 101 (2004) 367–372.
[12] S. Ookawara, R. Higashi, D. Street, K. Ogawa, Chem. Eng. J. 101 (2004) 171–178.
[13] J. Crank, The Mathematics of Diffusion, second ed., Clarendon Press, Oxford, 1975.
[14] H. Kawazumi, A. Tashiro, K. Ogino, H. Maeda, Lab Chip 2 (2002) 8–10.
[15] P.W. Atkins, Physical Chemistry, sixth ed., Oxford University Press, Oxford, 1998.
[16] D.J. LeCaptain, M.A. Michel, V.A. Orden, Analyst 126 (2001) 1279–1284.